HHS Public Access

Author manuscript

Chemistry. Author manuscript; available in PMC 2022 February 15.

Published in final edited form as:

Chemistry. 2021 February 15; 27(10): 3229–3237. doi:10.1002/chem.202003523.

High-Z metal-organic frameworks for X-ray radiation-based cancer theranostics

Megan J. Neufeld[a], **Alec Lutzke**[b], **Guillem Pratx**[c], **Conroy Sun**[a,d]

[a]Department of Pharmaceutical Sciences, College of Pharmacy, Oregon State University, Portland, OR 97201, United States

[b]Beckman Coulter Life Sciences, Loveland, CO 80538, United States

[c]Department of Radiation Oncology, Stanford University, Stanford, California 94305, United States

[d]Department of Radiation Medicine, Oregon Health & Science University, Portland, Oregon 97239, United States

Abstract

X-ray radiation is commonly employed in clinical practice for diagnostic and therapeutic applications. Over the past decade, developments in nanotechnology have led to the use of high-Z elements as the basis for innovative new treatment platforms that enhance the clinical efficacy of X-ray radiation. Nanoscale metal–frameworks (nMOFs) are coordination networks containing organic ligands that have attracted attention as therapeutic platforms in oncology and other areas of medicine. In cancer therapy, X-ray activated, high-Z nMOFs have demonstrated potential as radiosensitizers that increase local radiation dose deposition and generation of reactive oxygen species (ROS). This mini-review summarizes current research on high-Z nMOFs in cancer theranostics and discusses factors that may influence future clinical application.

Graphical Abstract

neufeldm@oregonstate.edu (M.J.N), sunc@ohsu.edu (C.S).

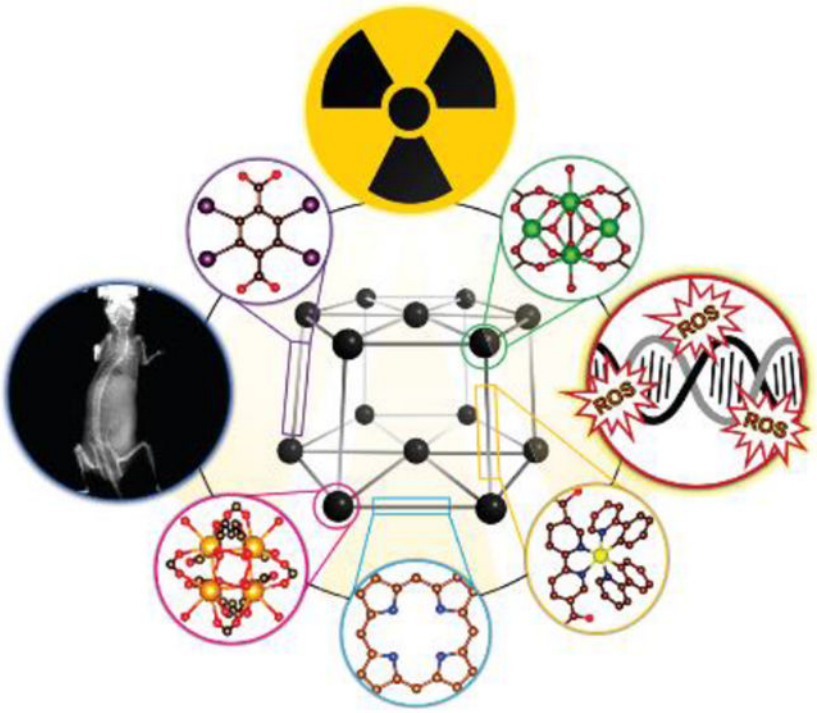

High-Z nanoscale metal–organic frameworks (nMOFs) have attracted attention in oncology as X-ray contrast agents and radiosensitizers that enhance the effect of radiation therapy.

Graphical Abstract

X-ray activated nanoscale metal–organic frameworks for cancer theranostics

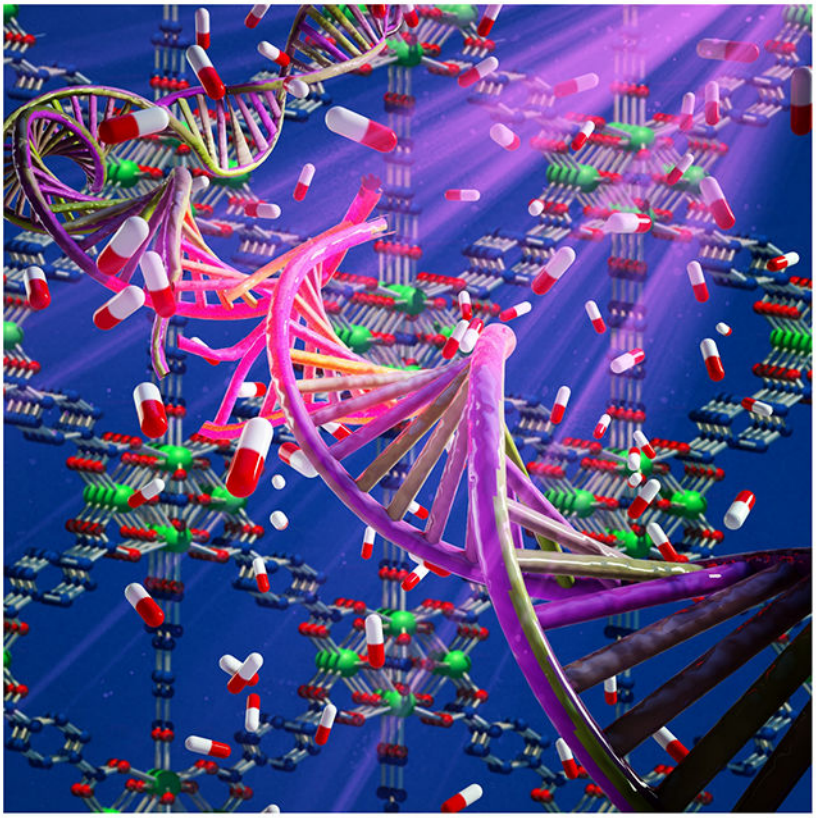

Keywords

radiation; cancer theranostics; metal–frameworks; nanomedicine; biomedical imaging

1. Introduction

In current clinical practice, X-ray radiation is routinely employed throughout patient care for applications ranging from diagnostics to radiation therapy (RT). These clinical procedures rely on unique phenomena arising from the interaction of high-energy radiation and matter. Within the diagnostic X-ray energy range, differential X-ray attenuation produces contrast for computed tomography (CT) and other imaging techniques.[1] In the case of RT, damage to cancer cells results from chemical effects produced by dissipation of ionizing radiation, including formation of genotoxic reactive oxygen species (ROS).[2] The conditional increase in radiation absorption as atomic number rises has led to the recruitment of so-called high-Z elements as critical tools for clinicians and platforms for innovative new treatments. For example, contrast between biological tissues in radiographic imaging is commonly improved through use of iodine (Z = 53) and barium (Z = 56) contrast agents. Furthermore, clinical trials have demonstrated that intratumoral hafnium (Z = 72) oxide nanoparticles (NPs) can be used to enhance the local effect of radiation therapy, illustrating the potential use of high-Z elements in cancer treatment.[3]

Over the last decade, interest has developed in harnessing the X-ray absorption and scattering properties of high-Z elements by incorporating them within nanoscale coordination polymers. Coordination polymers are a class of multi-dimensional materials constructed by connecting inorganic nodes (metal ions or clusters) and bridging organic linkers through coordination bonds. When the resulting structure is an open framework with potential void space, the term metal–organic framework (MOF) is often applied and will be used throughout this review (Figure 1a). Structurally diverse MOFs are accessible through variation of the metal (*e.g.*, d- and f-block elements) and organic linker (e.g., carboxylates and nitrogen heterocycles) to impart particular physical and chemical properties, leading to thousands of reported MOFs with unique features.[4] Straightforward crystal engineering allows for selective functionalization of MOFs and the integration of active secondary building units (SBUs). The size of a MOF may also be controllably restricted to the nanoscale regime during synthesis, and it is this property that has led to adaptation of MOFs in nanomedicine research. The evolution of nanoscale MOFs (nMOFs) has significantly expanded their potential as therapeutic platforms in oncology and other areas of medicine, where NPs have attracted attention in photodynamic therapy (PT), drug delivery, and imaging.[5] A more extensive overview of nMOFs for cancer theranostics and their design principles is provided elsewhere.[5] nMOFs containing high-Z elements have been proposed for use as radiosensitizing platforms for both increasing radiation dose deposition and enhancing local ROS generation.[6]

The unique structural and chemical characteristics of MOFs facilitate the incorporation of high-Z elements for imaging and cancer therapy. In many reported structures, high-Z elements such as zirconium (Z = 40) and hafnium are incorporated as metal centers that are integral to the framework itself (Figure 1b). In other cases, high-Z elements are covalently bound to the organic linkers, chelated by ligating functional groups, or hosted within the porous structure of the MOF (Figure 1b). Some structures have combined these approaches to incorporate high-Z elements. Organic linkers and high-Z elements may be rationally combined to achieve particular functions through cooperative mechanisms, including radioluminescence and enhanced radiosensitization. The porosity of nMOFs facilitates efficient storage and transport of therapeutic cargo, rendering them advantageous for combination therapies that have become common in oncology. Moreover, nMOFs are often biodegradable through hydrolytic and ligand exchange mechanisms and can be tuned for stability in biological environments by application of surface coatings. For these reasons, nMOFs are unique platforms for engineering X-ray responsive nanomaterials for cancer diagnostics and therapy. In this mini-review, we discuss the history and current state of the field and present factors that may influence future clinical adaptation.

2. Metal–frameworks for X-ray activated imaging applications

2.1. Computed tomography contrast agents

X-ray sources produce radiation from electrical energy by collision of electrons with a d-block metal anode.[7] This results in the emission of broad-spectrum radiation consisting of discrete, anode-dependent characteristic X-rays and continuous *Bremsstrahlung* radiation generated by deceleration of electrons.[1] Interaction of this incident radiation with matter

largely occurs through the photoelectric effect, Compton scattering, and pair production (Figure 2). In X-ray absorbance, critical maxima called absorbance edges result from the photoelectric effect. These edges correspond to the increased probability of photoelectron ejection from atomic electron shells (e.g., K, L, M) when the energy of incident photons is in excess of the electron binding energy. Due to the photoelectric effect, the mass attenuation coefficients of heavier elements are generally proportional to atomic number at diagnostic X-ray energies (20 to 150 keV).[1] For this reason, radiocontrast agents incorporate high-Z elements to improve attenuation relative to biological tissue. The earliest use of MOFs for this application was reported by deKrafft *et al.* in 2009, who synthesized copper(II) and zinc(II)-based 2,3,5,6-tetraiodo-1,4-benzenedicarboxylate MOFs for CT contrast.[8] Contrast was primarily conferred by the iodine-rich ligand, with copper (Z = 29) and zinc (Z = 30) contributing to approximately 5% of X-ray attenuation.[8]

UiO-66 (UiO: University of Oslo) is a 1,4-benzenedicarboxylate-based MOF architecture containing zirconium(IV) oxide nodes [$Zr_6O_4(OH)_4$] and exhibits exceptional water stability. The use of UiO-66 and its isostructural hafnium(IV) analog [UiO-66(Hf)] as potential CT contrast agents was introduced in 2012 by deKrafft et al., who reported the synthesis of several nanoscale variants (Figure 3a–c).[9] In these structures, the presence of zirconium and hafnium metal clusters provided contrast without the need for iodinated ligands. UiO-66(Hf) was coated with silica and polyethylene glycol (PEG) to produce nMOFs with improved physiological stability and biocompatibility. These nMOFs were evaluated by intravenous injection in mice, where accumulation in the liver and spleen suggested that MOF aggregation results in capture by the reticuloendothelial system. In 2017, Zhang et al. reported the use of post-synthetic exchange to replace 1,4-benzenedicarboxylate ligands in UiO-66 with a diiodo-monocarboxyl-substituted derivative of boron dipyrromethene (BODIPY).[10] Toxicity studies in mice did not discern any adverse effect at nMOF dosages as high as 0.1 mg g^{-1} body weight, while intravenous administration in an orthotopic hepatoma rat model yielded sufficient accumulation at the tumor site to provide CT contrast.

Multimodal imaging with MOFs has been demonstrated by Shang et al., who coated a gold nanorod core with a shell of the iron(III) fumarate MOF MIL-88A (MIL: Matériaux de l’Institut Lavoisier). This MOF was shown to selectively accumulate in the brain and liver after intravenous administration and provided contrast in CT, magnetic resonance imaging (MRI), and photoacoustic imaging (PAI) techniques.[11] In this case, the role of the MOF shell was primarily to prevent aggregation of the gold nanorod core. Zhang and colleagues fabricated a smart nMOF based platform for image-guided precise chemotherapy using 5-boronobenzene-1,3-dicarboyxlic (BBDC) acid with Yb^{3+} metal nodes.[12] X-ray CTs attenuation of the gastrointestinal tract increased approximately 5 - 90 minutes following administration with almost 100% of the Yb-BBDC nMOF being excreted within 24 hours. In 2019, Robison et al. introduced the use of bismuth-based 1,3,5,8-(p-benzoate)pyrene MOFs (Bi-NU-901) which demonstrated greater radiocontrast than the zirconium analogs for CT imaging, however their average size of 7 μm excludes intravenous use due to the risk of vascular occlusion.[13]

2.2. Radioluminescence

Certain nMOFs act as nanoscintillators by converting X-ray radiation into optical light. These nMOFs have potential application in new imaging techniques such as X-ray luminescence imaging and X-ray luminescence CT.[14] Compared to traditional inorganic scintillators, nMOFs may prove advantageous as theranostic materials due to their ability to incorporate molecular therapeutics, contrast agents, and ROS generating species, in tandem. Conjugation of these radioluminescent nMOFs with biological targeting agents could aid in identifying molecular signatures of biological or disease processes through imaging.[15] In 2014, Wang et al. synthesized hafnium(IV) and zirconium(IV)-based 9,10-anthracenyl bis(benzoate) MOFs for luminescence. They proposed that absorption of X-rays by hafnium and zirconium metal centers produces photoelectrons that subsequently excite the ligands and result in emission of visible light. Solvent molecules were found to affect luminescence. This work refrained from proposing a specific application for these luminescent materials. In 2017, Xie et al. demonstrated that a photoluminescent three-dimensional framework could be prepared from the uranyl cation and oxalate and succinate ligands.[16] Both X-rays and gamma-rays induced luminescence from this material. This material was proposed as a means of detecting ionizing radiation. In 2020, Neufeld et al. proposed europium and terbium-based 1,4-benzenedicarboxylic acid (BDC) nMOFs as molecular contrast probes for X-ray luminescence imaging.[17] Following X-ray excitation, all nMOFs displayed bright radioluminescence within the visible spectrum derived from the lanthanide metal (Figure 4a). For example, examination of the EuBDC emission spectra reveals characteristic Eu^{3+} emission at approximately 582, 593, 616, 654, and 702 nm (Figure 4b). The Ln-nMOFs retained their X-ray luminescence following cellular incubation and uptake, demonstrating their *in vitro* potential as radioluminescent cell labelling probes. (Figure 4c).

3. Metal–frameworks in radiation therapy

3.1. Radiation therapy

Low energy (less than 20 keV) photons are easily absorbed by low-Z elements in human tissue, have poor penetration depth, and consequently increase the effective surface dose with limited utility. In diagnostic or therapeutic applications, these photons are often removed by filtration. Medical linear accelerators used in RT deliver a high energy spectrum (up to 25 MeV).[1] Upon interaction with tissue, incident X-rays may be absorbed by ejection of an inner-shell electron, inelastically scattered by atomic electron clouds, or converted to an electron and positron. These phenomena and subsequent processes (e.g., Auger decay) generate numerous electrons and secondary X-rays of lower energy that result in excitation and ionization of chemical species. In RT, high energy particles may interact directly with various cellular components or indirectly through formation of ROS to induce DNA damage.[1–2] Because high-Z elements increase the likelihood of X-ray absorption and scattering, their presence intratumorally may result in local improvements to therapeutic efficacy without requiring higher radiation doses. For example, hafnium oxide NPs are currently undergoing clinical trials for augmenting RT with anti-PD1 in patients with advanced cancers.[3]

In clinical oncology, an estimated 60% of cancer patients receive RT, which is used as a primary treatment and in combination with other therapeutic intervention.[18] However, RT does not discriminate between healthy and diseased tissue. Consequently, RT must balance killing tumor cells without incurring significant collateral damage to surrounding healthy tissue. In addition to intrinsic limitations associated with severe radiation toxicity, the local tumor microenvironment (TME) can increase cancer cell radioresistance, requiring unsafe radiation doses for complete eradication.[19] The hypoxic nature of the TME can minimize cancer cell sensitivity to radiation, while elevated levels of antioxidants are highly effective at scavenging ROS.[20] For these reasons, RT alone is often inadequate for complete cancer remission and combination treatments that include surgery or chemotherapeutics are often required.

3.2. Metal–organic frameworks for enhanced radiation therapy

The porosity and large surface area of many MOF architectures led to their proposed use as drug delivery vehicles for chemotherapeutics and other molecules.[21] More recently, the tunability of MOFs has encouraged the rational design of stimulus responsive nMOFs through incorporation of heavy elements and functional ligands. This has resulted in the pursuit of nMOFs as stimulus-responsive materials in photodynamic therapy (PDT). PDT is based on the ability of photosensitizers (e.g., porphyrins) to generate highly reactive singlet oxygen ($^1O_2$) following energy specific light activation.[22] Following the initial demonstration of porphyrin-based nMOFs for PDT in 2014, there has been significant progress in this area that is comprehensively reviewed elsewhere.[23] In 2016, the rational design of nMOFs for combined PDT and RT was first reported by Liu *et al.* Here, Hf-TCPP was synthesized using hafnium metal centers and the commercially available photosensitizer, tetrakis(4-carboxyphenyl) porphyrin (TCPP), as the organic linker.[24] Incorporation of the high-Z element hafnium enhanced interactions with ionizing radiation that ultimately produces cytotoxic ROS, while the photosensitizing ligand TCPP resulted in $^1O_2$ formation upon exposure to tissue-penetrating 661 nm (1.88 eV) light. Anti-cancer efficacy in a 4T1 murine breast cancer model demonstrated that the combined treatment of intravenously administrated Hf-TCPP with RT and PDT significantly improved tumor regression, demonstrating the potential of high-Z nMOFs for enhancing RT. This carboxylate nMOF is hydrolytically sensitive and decomposes over time to permit efficient clearance, unlike inorganic high-Z NPs

3.3. Metal–organic frameworks for RT and X-ray photodynamic therapy

Tumor hypoxia and low tissue penetration of light are often cited as limitations of PDT, which relies on direct excitation of a photosensitizer in the presence of molecular oxygen to produce a therapeutic effect. These limitations are partially ameliorated in X-ray PDT (often termed X-PDT or *radiodynamic therapy*), a technique used by Lin et al. to harness the properties of dimensionally constrained MOFs called metal–organic layers (MOLs).[25] In this approach, hafnium metal centers are used to simultaneously generate hydroxyl radicals and enable X-ray PDT by absorbing and transferring energy to various photosensitizing ligands to generate $^1O_2$ and superoxide anions (O_2^-).[25–26] The mechanism of X-ray PDT has not been clearly elucidated and is likely distinct from that of PDT.[27] In the traditional description of ROS generation by photosensitization, the triplet excited state (T_1) of the

photosensitizer is the critical intermediate in both Type I (O_2^--forming) and Type II ($^1O_2$-forming) reactions.[23b]

Despite enhanced permeability and retention (EPR), low tumoral NP accumulation remains a major limitation of clinical applications via intravenous administration. To overcome these limitations, various approaches have been investigated for further enhancing NP-based radiosensitization. This concept was recently expanded on by Lan et al. by encapsulating Wells-Dawson type polyoxometalates (POMs, W_{18}) with a Hf-based MOF (Hf_{12}-DBB-Ir) through electrostatic interactions (Figure 5a). The incorporation of POMs was used to improve $^{\bullet}OH$, $^1O_2$, and O_2^- generation, by radiolysis, photosensitizing, and redox-activation, to synergistically enhance anticancer efficacy.[28] To overcome tumor hypoxia, nMOFs have been engineered to increase the efficacy of RT in low oxygen (O_2) environments. These nMOFs exploit the high intratumoral levels of H_2O_2 by incorporating redox-active metals (Mn, Cu, and Fe) capable of catalytically decomposing H_2O_2 into $^1O_2$/$^{\bullet}OH$ or inhibiting signaling pathways that increase tumoral H_2O_2 pathways.[29] A recent report by Gong et al. proposed dual RT and chemodynamic therapy (CDT) through the incorporation of Fe^{3+} into Hf nMOFs (Hf-BPY-Fe) could catalyze $^{\bullet}OH$ production from endogenous H_2O_2 through the Fenton reaction.[29c] These NPs both increase cancer cell susceptibility to RT through continuous catalytic generation of intracellular ROS and further enhances radiation dose deposition, thus working synergistically to promote tumor control in a process referred to as full process radiosensitization (Figure 5b).

3.4. Metal–organic frameworks for immuno-radiotherapy

Cancer immunotherapies such as checkpoint blockade immunotherapy (CBI) have become an important treatment modality particularly in combination with RT. CBI works by employing the immune system through stimulation of T cells to recognize and attack tumor cells, thus enhancing the systemic antitumor immune response. In addition to inducing DNA damage, RT has been shown to induce an immunomodulatory response and synergize with checkpoint blockade. Moreover, the observations of hafnium nMOFs to synergize with immunotherapies and the known ability of X-ray stimulated HfO_2 NPs to activate the cGAS-STING pathway makes these materials highly attractive approaches for improving the efficacy of immunotherapy by priming the anti-tumor response.[30] The Lin group, in particular, has established the feasibility of combining Hf-based nMOFs with RT-RDT and anti-PD-L1 antibody or small molecule IDO inhibitor.[31] Synergistic combinations of Hf-nMOFs with checkpoint blockade inhibitors led antitumor efficacy in both local and distant tumor regression due to systemic antitumor efficacy. In a recent report, Ni and colleagues found that the synergistic combination of CBI, RT, and Hf-MOLs, based on $Hf_{12}O_8(OH)_{14}$ SBUs and photosensitizing ligands (5,15-di(p-benzoato)porphyrin), resulted in both antitumor efficacy and antimetastatic effects in a lung metastatic triple negative breast cancer model (Figure 6).

3.5. Metal–organic frameworks for chemoradiotherapy

In addition to their radiation enhancing properties, the high porosity of MOFs facilitates efficient storage and transport of many different chemotherapeutics. These inherent properties can be exploited to engineer nMOF platforms that simultaneously increase the

effective radiation dose and deliver radiosensitizing drugs, thus leading to improve therapeutic efficacy. However, these combined therapeutic routes remain relatively unexplored.[33] In 2017, the Liu group demonstrated the potential of NCPs as novel chemoradiation platforms. In the first report, MnO_2 NPs were stabilized in bovine serum albumin and encapsulated in NCP-shells composed of Hf and the synthesized prodrug of the chemotherapeutic cisplatin, c,c,t-(diamminedichlorodisuccinato (DSP)) Pt(IV), (BM@NCP(DSP)-PEG.[33a] In the second study, Hf ions were coordinated with the synthesized benzoic-imine linker and loaded with the chemotherapeutic drug chloro(triphenylphosphine)gold(I) (TPPGC) to form NCPs.[33b] These accounts demonstrated the synergistic combination of NCPs + RT treatment for significantly inhibiting tumor growth compared to drug + RT controls. Collectively, these reports establish the potential design of NCP platforms for combined chemotherapy and RT. In 2019 Neufeld et al. utilized the Hf-analog of UiO-66 (Hf-BDC) for co-delivery of two DNA damage repair inhibitors (DDRis).[34] Compared to traditional chemotherapeutics, DDRi's target the signaling and repair mechanisms of associated with DNA damage. Here, the Hf-UiO-66 was synthesized followed by PEGylation and drug loading with talazoparib (T) and buparlisib (B) to obtain (TB@Hf-BDC-PEG) (Figure 7a). In vitro quantification of induced DNA damage via γ-H2AX assay revealed that 24 h after radiation, most of the DNA damage disappeared in the control group and Hf-BDC-PEG, indicative of efficient DNA repair (Figure 7b). Comparatively, a significant portion of foci remained after 24 h in the TB@Hf-BDC-PEG group suggesting inhibition or failure of the DNA damage induced by Hf-BDC-PEG. Overall, this report demonstrates the synergistic combination of DDRi's and Hf-nMOFs for enhancing the therapeutic efficacy of RT by both enhancing DNA damage and inhibiting repair (Figure 7c).

4. Discussion

4.1. Radiation adsorption and enhancement in high-Z metal–organic frameworks

Studies evaluating the anti-cancer efficacy of high-Z nMOFs in X-ray PDT and related combination therapies have produced promising *in vivo* results. However, many mouse and rat RT models have utilized a comparatively low energy X-ray spectrum (120 to 225 kVp accelerating potentials) that is strongly attenuated by photoelectric absorption in hafnium and other elements with similar K-edge energies (65 keV).[26a, 28, 31a, 32] Only three reports have used clinically relevant energies in high-Z MOF RT experiments, a factor that may hinder direct clinical translation.[29c, 33] Megavoltage radiation emitted by clinical linear accelerators interacts with matter via Compton scattering and pair production, and only the latter phenomenon is proportional to atomic number. Compton scattering itself is proportional to electron density, and the probability of this interaction is greater in high density (ρ) materials. The substantial bulk density of heavy metals may be largely irrelevant in low-density MOFs (UiO-66 density ranges from 0.430 – 1.24 g cm^{-3}, depending on porosity) that contain these high-Z elements as individual atoms or small polyatomic clusters.[35] When normalizing for the influence of density, there are only modest differences in X-ray energy transfer as a function of effective atomic number at energies within the Compton scattering regime. For example, the mass energy-absorption (μ_{en}/ρ) coefficient of elemental hafnium at 1 MeV (3.2×10^{-2} cm^2 g^{-1}) is just 3% greater than that of water (3.1 ×

10^{-2} cm^2 g^{-1}). In contrast, the value is over 80-fold greater for hafnium (2.1 cm^2 g^{-1}) when compared to water (2.5×10^{-2} cm^2 g^{-1}) at 100 keV.[35] The energy dependence of X-ray absorption phenomena may partially account for the mixed effects on *in vivo* growth observed in certain high-energy RT models. [29] Taken as a whole, the most significant interaction between high-Z MOFs and radiation is likely from photoelectric absorption.

NP-based dose enhancement is not uniform in space, and greater enhancement effects are achieved when NPs are in close proximity (~0.5 nm) to their biological target. It has been hypothesized that radioenhancement in hafnium-based MOFs is promoted by efficient capture of secondary photons by tightly spaced, periodic hafnium clusters in the crystalline lattice. [31b] However, this phenomenon has yet to be verified and may be unlikely due to the low chance of secondary photon interaction within a nanoscale structure. The porous structure of MOFs offers substantial surface area for generation of radicals from water and oxygen and may facilitate rapid diffusion of short-lived ROS into surrounding tissue.[32] Low energy (120 kVp) mouse tumor regression and hydroxyl radical generation studies indicate that hafnium can exhibit greater radioenhancement efficiency *per mole* in MOFs when compared with hafnium oxide NPs.[31b] .

Formation of ROS via the X-ray photochemistry of metals has been discussed in detail elsewhere.[36] The role of certain porphyrin-based ligands in X-ray PDT is less clearly understood from a mechanistic perspective, but is likely to involve ligand excitation or ionization by electrons or secondary photons produced from the interaction of radiation with metal centers. The ligand triplet state is then populated by intersystem crossing or ion recombination and ROS are formed following known photosensitization processes.[37] Predictably, the design of MOFs for X-ray PDT has largely been dependent on adaptation of structures that function in traditional PDT.

4.2. Stability

In most medical applications, MOFs are expected to degrade by hydrolysis or interaction with biomolecules following intravenous or intratumoral administration. However, MOF degradation prior to use is undesirable and may be difficult to control in clinical formulations. Existing intravenous iodinated radiocontrast agents (e.g., Iohexol) are used and sold as ready-to-inject aqueous solutions with storage lives of years. In contrast, even robust MOFs such as UiO-66 degrade in water and their stability is rarely characterized beyond durations of days or weeks.[38] While storage stability can be improved with post-synthetic modification, these more durable MOFs may resist clearance.

4.3. Toxicity

In high-Z MOFs designed for RT, stimulus-triggered, localized cytotoxicity is a desirable property, while persistent, systemic toxicity is not. Due to the aqueous instability of MOFs, degradation products are a possible source of systemic toxicity. The ability to directly test MOF degradation products for toxicity is limited by the fact that the pharmacokinetics of high-Z MOFs are largely unknown. It is often assumed that *in vivo* MOF degradation results in release of the direct precursors (*i.e.*, metal ions and organic ligand), yet certain MOFs may undergo structural rearrangements or reactions that generate new inorganic species with

potential adverse side effects.[39] Moreover, the porosity and large surface area of MOFs render them uniquely susceptible to persistent contamination by impurities, including toxic solvents such as *N*,*N*-dimethylformamide (DMF).[40]

In any discussion of metal-based therapeutics, it is obligatory to consider the possibility of metal toxicity. Group 4 metals are often considered to have minimal toxicity, although this broad assertion does not account for substantial variability in metal toxicity depending on oxidation state and ligation.[41] There is evidence that titanium and zirconium ions may cross the cell membrane and produce deleterious biological effects through ROS generation.[41a] While the general toxicity of hafnium has rarely been studied, existing *in vitro* and *in vivo* studies generally do not support significant toxicity for high-Z nMOFs.[42]

4.4. Administration and tumor accumulation

For radiocontrast applications, intravenous injection of nMOFs and tissue-selective deposition has been reported in multiple studies.[8–11] The efficacy of high-Z MOFs for enhanced RT has been demonstrated using intratumoral injection as the route of administration. While local administration ensures high NP accumulation and is optimal for increasing therapeutic efficacy in RT, it is often not feasible in clinical scenarios. Gong et al. observed that *intravenous* administration of the hafnium-based nMOF Hf-BPY-Fe did not improve tumor growth control compared to RT alone, an outcome attributed to low NP accumulation in tumors.[29c] Modification of the Hf-BPY-Fe particles via PEG increased blood half-life, tumor accumulation, and to some extent suppress tumor growth. Hafnium accumulation was increased in nearly all organs demonstrating the lack of PEG coating for selectively promoting tumor accumulation. Moving forward, approaches that enhance tumoral nMOF accumulation, such as targeted surface modification, may aid in enhancing the therapeutic efficacy of intravenous administration.

5. Summary and Outlook

The unique structural characteristics of high-Z MOFs confer the ability to design diagnostic or therapeutic materials for X-ray medicine. While nMOFs may offer advantages in cancer treatment that outweigh stability concerns, there are fewer apparent benefits for imaging applications. Practicality is crucial in the effective clinical translation of nanomaterials. It is important that patient needs and manufacturability guide the development of medical MOF technologies rather than novelty. From an industrial standpoint, clinical translation of nMOFs will be highly dependent on the development of straightforward and reliable synthetic protocols and characterization techniques. In general, these discussed factors highlight our current lack of understanding regarding the fundamental physical and chemical processes for nMOF induced radioenhancement. Further understanding of the parameters that influence enhancement (*e.g.* dose rate, energy transfer, X-ray energy, and ROS generation) will prove critical towards the fine-tuning nMOF platforms for X-ray based techniques. A critical step towards accurate therapeutic representation should involve focusing on using clinical energies or pre-clinical energies that best mimic clinical tumor response.

Acknowledgements

This work was supported by the NIH NIGMS as a Maximizing Investigators' Research Award 1R35GM119839-01 (C.S.)

Biographies

Megan J Neufeld received her Ph.D. in chemistry from Colorado State University under the supervision of Prof. Melissa Reynolds in 2018. She received her bachelor's degree at Southern Oregon University. Currently she is working as a postdoctoral scholar at Oregon State University under the advisory of Prof. Conroy Sun. Her research focuses on developing novel nMOF platforms for drug delivery, radiation enhancement, and molecular imaging in cancer treatment.

Alec Lutzke completed his Ph.D. at Colorado State University (CSU) under the supervision of Prof. Melissa M. Reynolds. His research focused on the synthesis of materials for medical applications. He is currently a development scientist at Beckman Coulter Life Sciences (Loveland, CO).

Guillem Pratx, Ph.D. is Assistant Professor of Radiation Oncology and Medical Physics at Stanford University. The physical Oncology Lab, which he leads, employs physics and math to advance cancer research and patient care. Research projects blend traditional medical physics concepts with recent advances in biomedical engineering to incorporate novel capabilities into current medical imaging and enhance radiation therapy processes. Prof. Pratx is a Damon Runyon Innovator, an SNMMI Young Investigator, an NIH Investigator, and the author of over 70 publications.

Conroy Sun, Ph.D. is an Assistant Professor of Pharmaceutical Sciences at Oregon State University. He is also Affiliate Assistant Professor of Radiation Medicine and a member of the Knight Cancer Insitiute at Oregon Health & Science University. Dr. Sun's Lab is focused

on developing biomaterials for drug delivery and molecular imaging with an emphasis on applying nanotechnology in medicine. His research, which has been funded by the NIH and DOD, is reported in over 50 publications and has been cited over 7000 times.

References

[1]. Kuncic Z, Lacombe S, Phys. Med. Biol 2018, 63, 02TR01.

[2]. Fu PP, Xia Q, Hwang H-M, Ray PC, Yu H, J. Food Drug Anal 2014, 22, 64–75. [PubMed: 24673904]

[3]. Shen C, Jameson K, Weiss J, Hackman T, Corum D, Akulian JA, Dixon R, Pearson A, Frakes J, Said P, Miraoui H, Baskin-Bey E, Seiwert T, Annals of Oncology 2019, 30.

[4]. Safaei M, Foroughi MM, Ebrahimpoor N, Jahani S, Omidi A, Khatami M, TrAC, Trends Anal. Chem 2019, 118, 401–425.

[5]. Sun WJ, Li SY, Tang GL, Luo Y, Ma SJ, Sun SX, Ren JB, Gong Y, Xie CH, Int. J. Nanomed 2019, 14, 10195–10207;(b)Lu KD, Aung T, Guo NN, Weichselbaum R, Lin WB, Adv. Mater 2018, 30.

[6]. Ni K, Lan G, Lin W, ACS Cent. Sci 2020**,** 6, 861–868.**,**

[7]. Lusic H, Grinstaff MW, Chem. Rev 2013, 113, 1641–1666. [PubMed: 23210836]

[8]. Dekrafft KE, Xie ZG, Cao GH, Tran S, Ma LQ, Zhou OZ, Lin WB, Angew. Chem., Int. Ed 2009, 48, 9901–9904.

[9]. deKrafft KE, Boyle WS, Burk LM, Zhou OZ, Lin WB, J. Mater. Chem 2012, 22, 18139–18144. [PubMed: 23049169]

[10]. Zhang T, Wang L, Ma C, Wang WQ, Ding J, Liu S, Zhang XW, Xie ZG, J. Mater. Chem. B 2017, 5, 2330–2336. [PubMed: 32263624]

[11]. Shang WT, Zeng CT, Du Y, Hui H, Liang X, Chi CW, Wang K, Wang ZL, Tian J, Adv. Mater 2017, 29, 1604381.

[12]. Zhang H, Shang Y, Li YH, Sun SK, Yin XB, ACS Appl. Mater. Interfaces 2019, 11, 1886–1895. [PubMed: 30584757]

[13]. Robison L, Zhang L, Drout RJ, Li P, Haney CR, Brikha A, Noh H, Mehdi BL, Browning ND, Dravid VP, Cui Q, Islamoglu T, Farha OK, ACS Appl. Bio Mater 2019, 2, 1197–1203.

[14]. Klein JS, Sun C, Pratx G, Phys. Med. Biol 2019, 64, 04TR01.

[15]. Carpenter CM, Sun C, Pratx G, Liu HG, Cheng Z, Xing L, Opt. Express 2012, 20, 11598–11604. [PubMed: 22714145]

[16]. Xie J, Wang YX, Liu W, Yin XM, Chen LH, Zou YM, Diwu J, Chai ZF, Albrecht-Schmitt TE, Liu GK, Wang SA, Angew. Chem., Int. Ed 2017, 56, 7500–7504.

[17]. Neufeld MJ, Winter H, Landry MR, Goforth AM, Khan S, Pratx G, Sun C, ACS Appl. Mater. Interfaces 2020, 12, 26943–26954.

[18]. Schaue D, McBride WH, Nat. Rev. Clin. Oncol 2015, 12, 527–540. [PubMed: 26122185]

[19]. Kwatra D, Venugopal A, Anant S, Transl. Cancer Res 2013, 2, 330–342.

[20]. Brown JM, William WR, Nat. Rev. Cancer 2004, 4, 437–447. [PubMed: 15170446]

[21]. Wu MX, Yang YW, Adv. Mater 2017, 29, 1606134.

[22]. Dolmans DEJGJ, Fukumura D, Jain RK, Nat. Rev. Cancer 2003, 3, 380–387. [PubMed: 12724736]

[23]. (a)Lan G, Ni K, Lin W, Coord. Chem. Rev 2019, 379, 65–81; [PubMed: 30739946] (b)Lismont M, Dreesen L, Wuttke S, Adv. Funct. Mater 2017, 27, 1606314.

[24]. Liu JJ, Yang Y, Zhu WW, Yi X, Dong ZL, Xu XN, Chen MW, Yang K, Lu G, Jiang LX, Liu Z, Biomaterials 2016, 97, 1–9. [PubMed: 27155362]

[25]. Lan GX, Ni KY, Xu RY, Lu KD, Lin ZK, Chan C, Lin WB, Angew. Chem., Int. Ed 2017, 56, 12102–12106.

[26]. (a)Ni KY, Lan GX, Veroneau SS, Duan XP, Song Y, Lin WB, Nat. Commun 2018, 9, 4321; [PubMed: 30333489] (b)Lan GX, Ni KY, Veroneau SS, Song Y, Lin WB, J. Am. Chem. Soc 2018, 140, 16971–16975. [PubMed: 30485084]

[27]. Sun WJ, Zhou ZJ, Pratx G, Chen XY, Chen HM, Theranostics 2020, 10, 1296–1318.

[28]. Lan GX, Ni KY, Veroneau SS, Luo TK, You E, Lin WB, J. Am. Chem. Soc 2019, 141, 6859–6863. [PubMed: 30998341]

[29]. (a)Ma TC, Liu YD, Wu Q, Luo LF, Cui YL, Wang XH, Chen XW, Tan LF, Meng XW, ACS Nano 2019, 13, 4209–4219; [PubMed: 30933559] (b)Chen YY, Zhong H, Wang JB, Wan XY, Li YH, Pan W, Li N, Tang B, Chem. Sci 2019, 10, 5773–5778; [PubMed: 31293764] (c)Gong T, Li Y, Lv B, Wang H, Liu Y, Yang W, Wu Y, Jiang X, Gao H, Zheng X, Bu W, ACS Nano 2020, 14, 3032–3040.

[30]. Marill J, Anesary NM, Paris S, Radiother. Oncol 2019, 141, 262–266. [PubMed: 31439450]

[31]. (a)Lu K, He C, Guo N, Chan C, Ni K, Lan G, Tang H, Pelizzari C, Fu Y-X, Spiotto MT, Weichselbaum RR, Lin W, Nat. Biomed. Eng 2018, 2, 600–610; [PubMed: 31015630] (b)Ni KY, Lan GX, Chan C, Quigley B, Lu KD, Aung T, Guo NN, La Riviere P, Weichselbaum RR, Lin WB, Nat. Commun 2018, 9, 2351. [PubMed: 29907739]

[32]. Ni K, Lan G, Chan C, Duan X, Guo N, Veroneau SS, Weichselbaum RR, Lin W, Matter 2019, 1, 1331–1353. [PubMed: 32832885]

[33]. (a)Liu JJ, Chen Q, Zhu WW, Yi X, Yang Y, Dong ZL, Liu Z, Adv. Funct. Mater 2017, 27, 1605926;(b)Liu JJ, Wang HR, Yi X, Chao Y, Geng YH, Xu LG, Yang K, Liu Z, Adv. Funct. Mater 2017, 27,1703832

[34]. Neufeld MJ, DuRoss AN, Landry MR, Winter H, Goforth AM, Sun C, Nano Research 2019, 12, 3003–3017.

[35]. Goldsmith J, Wong-Foy AG, Cafarella MJ, Siegel DJ, Chem. Mater2013, 25, 3373–3382.

[36]. Stumpf V, Gokhberg K, Cederbaum LS, Nat. Chem2016, 8, 237–241. [PubMed: 26892555]

[37]. DeRosa MC, Crutchley RJ, Coord. Chem. Rev 2002, 233, 351–371.

[38]. Burtch NC, Jasuja H, Walton KS, Chem. Rev 2014, 114, 10575–10612. [PubMed: 25264821]

[39]. Simon-Yarza T, Mielcarek A, Couvreur P, Serre C, Adv. Mater 2018, 30, 1707365.

[40]. Sajid M, Environ. Sci. Pollut. Res 2016, 23, 14805–14807.

[41]. (a)Cossellu G, Motta V, Dioni L, Angelici L, Vigna L, Farronato G, Pesatori AC, Bollati V, Plos One 2016, 11, e0161916 ; [PubMed: 27611787] (b)Soto-Alvaredo J, Blanco E, Bettmer J, Hevia D, Sainz RM, López Cháves C, Sánchez C, Llopis J, Sanz-Medel A, Montes-Bayón M, Metallomics 2014, 6, 1702–1708. [PubMed: 25001216]

[42]. (a)Field JA, Luna-Velasco A, Boitano SA, Shadman F, Ratner BD, Barnes C, Sierra-Alvarez R, Chemosphere 2011, 84, 1401–1407; [PubMed: 21605889] (b)Yuan S, Qin J-S, Lollar CT, Zhou H-C, ACS Cent. Sci 2018, 4, 440–450. [PubMed: 29721526]

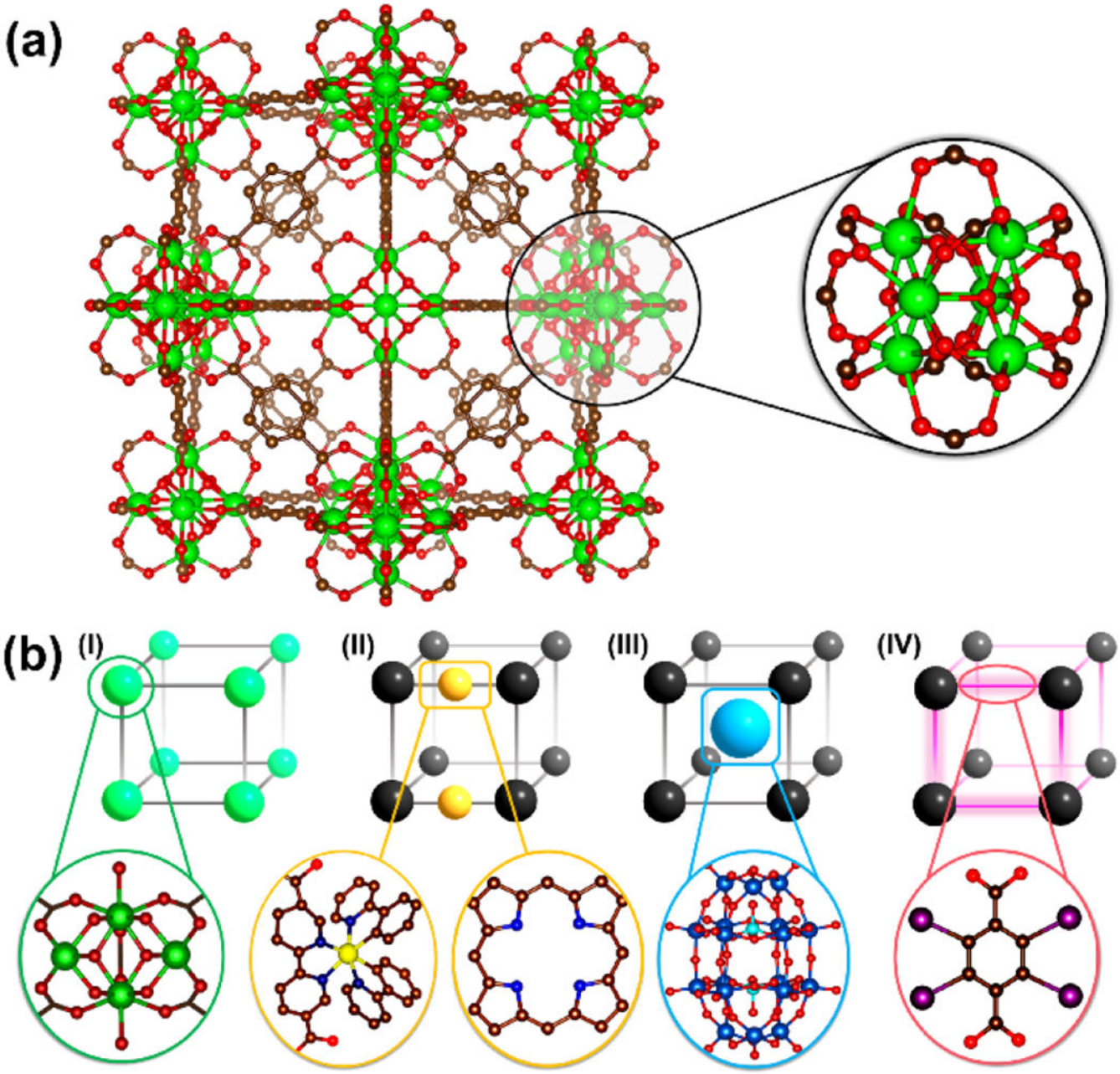

Figure 1.

(a) Structure of UiO-66 and local environment around the metal centers that forms the secondary building units (SBU). **(b)** Schematic illustration showing the strategies of incorporating high-Z X-ray responsive elements into nMOFs; (I) direct incorporation of relevant metal as connecting points, (II) chelation by organic linkers, (III) hosting as guest within the porous framework, and (IV) covalent attachment to the organic linkers.

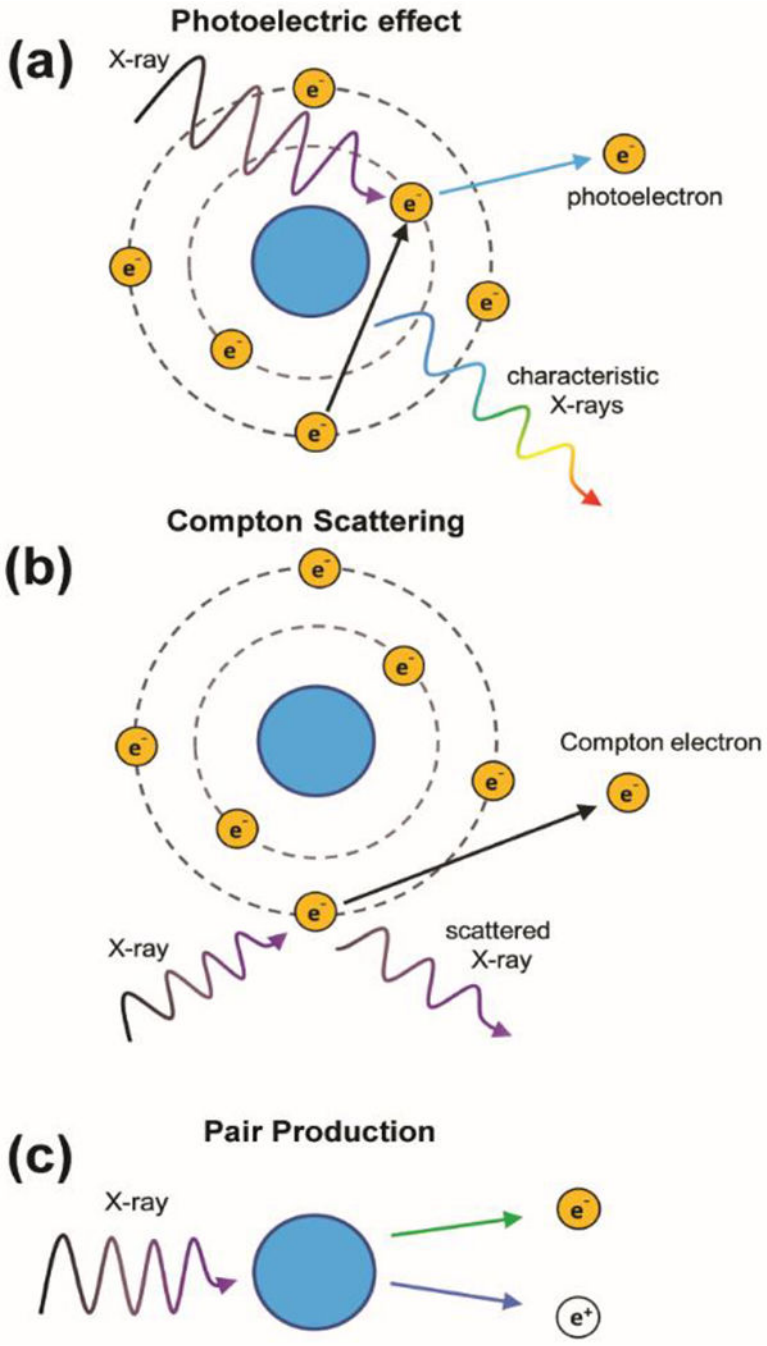

Figure 2.
Illustrations of processes that may occur when X-rays interact with atoms.

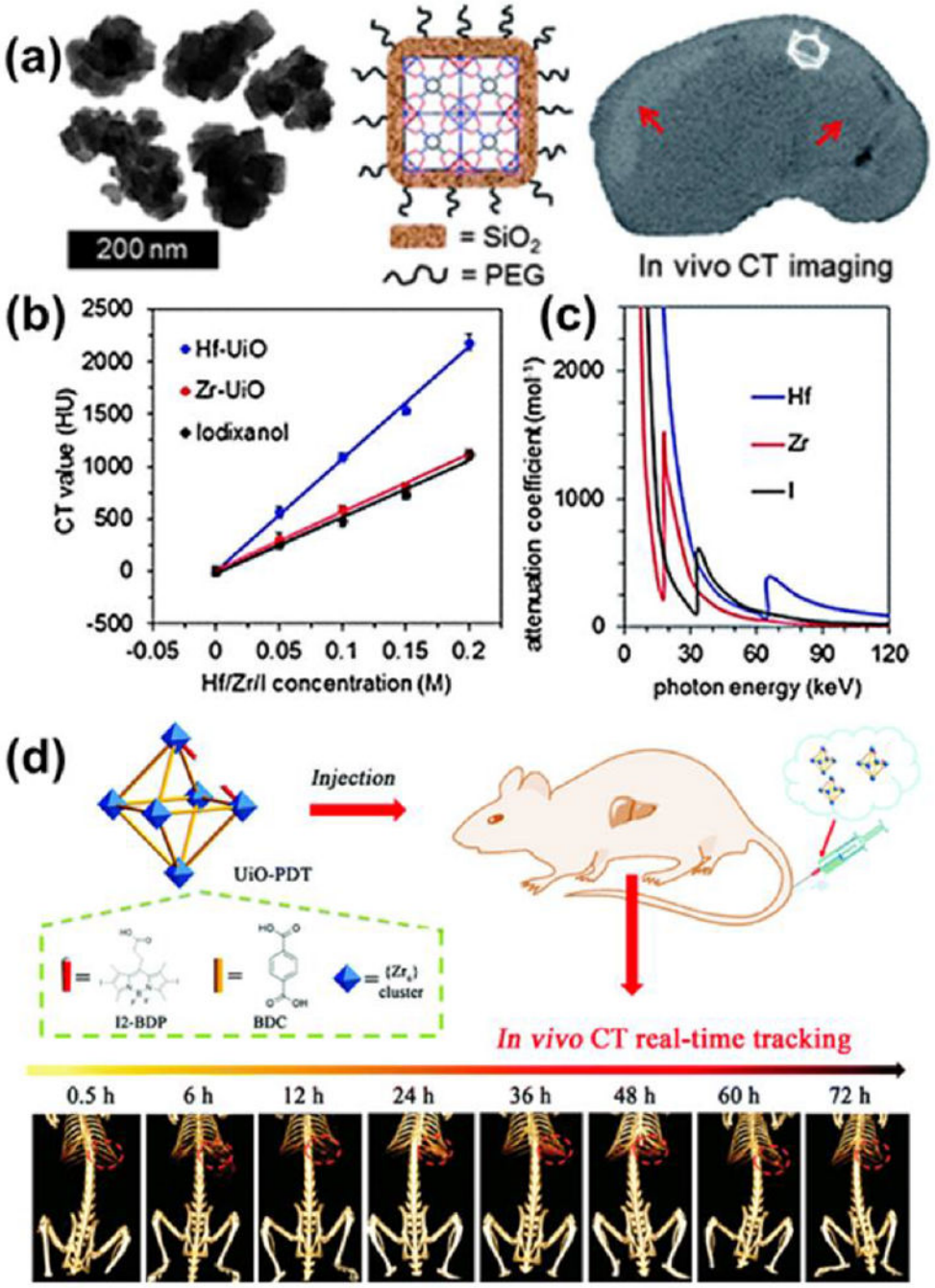

Figure 3.

(a) Schematic illustration of Hf-NMOF@SiO_2@PEG nMOF for CT imaging **(b)** X-ray attenuation as a function of [Hf/Zr/I] and **(c)** attenuation coefficient vs. photon energy. Adapted with permission.[9] **(d)** Schematic illustration of the synthesis of UiO-PDT nMOF and their in vivo X-ray CT imaging application.[10] Adapted with permission. Copyright 2020, Royal Society of Chemistry.

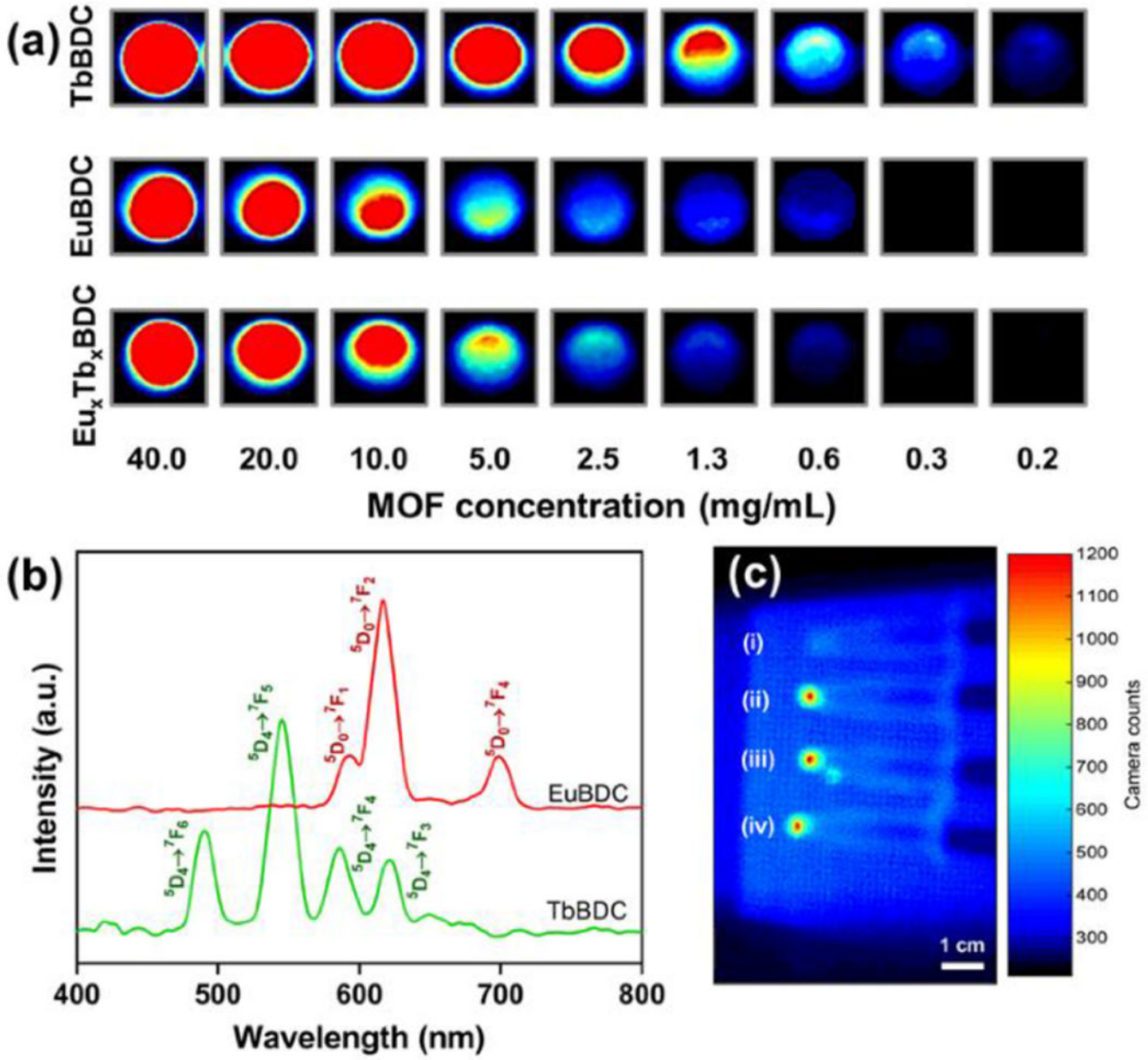

Figure 4.

(a) RL emission spectrum and **(b)** RL imaging of TbBDC-PEG, EuBDC-PEG, and EuxTbxBDC-PEG nMOF concentrations (mg/mL) in H_2O. **(c)** *In vitro* RLI of CT26 cell pellets under X-ray excitation of (i) blank cells and cells incubated with (ii) EuBDC-PEG, (iii) TbBDC-PEG, and (iv) EuxTbxBDC-PEG nMOFs for 24 h. Adapted with permission.[17] Copyright 2020, American Chemical Society.

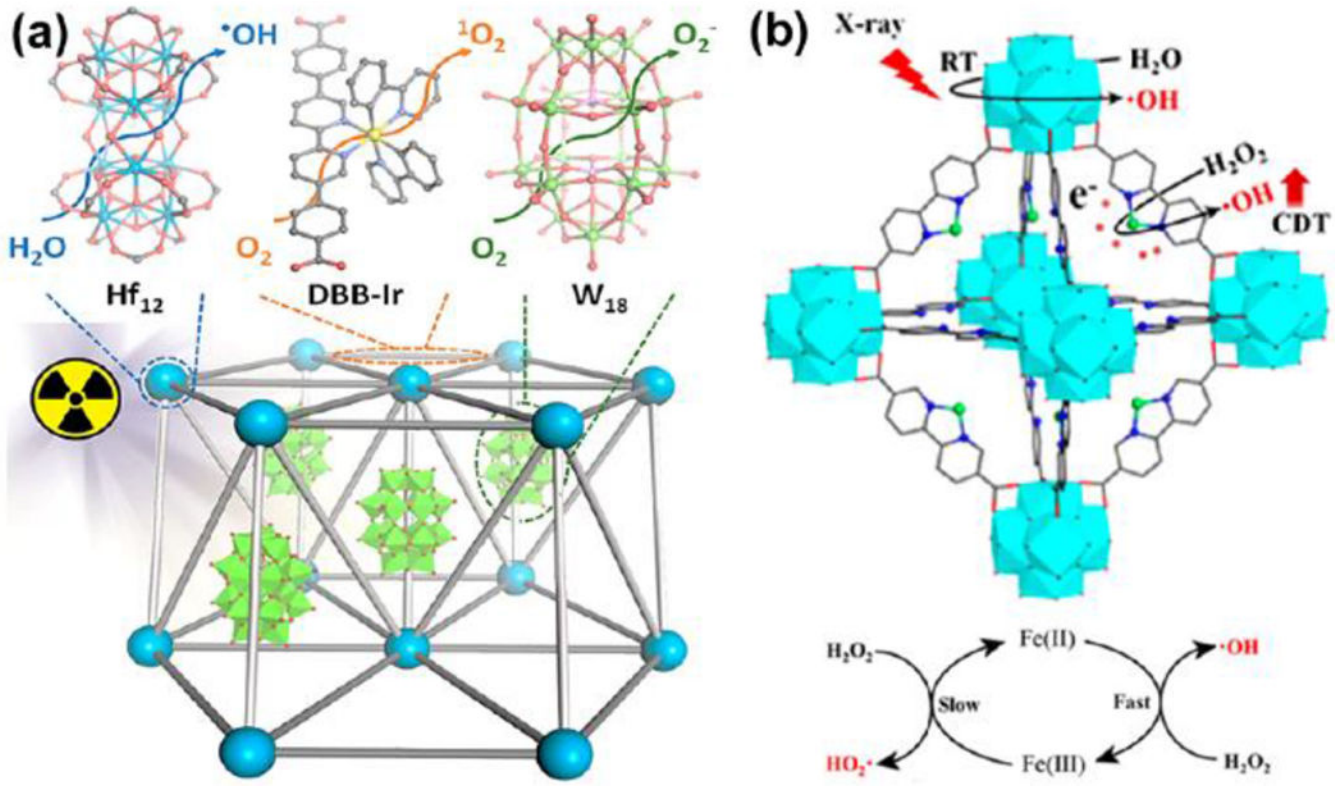

Figure 5.

(a) Assembly of Hf_{12}DBB-Ir, and W_{18} subunits in W_{18}@Hf_{12}-DBB-Ir to generate three distinct ROSs upon X-ray irradiation [28] and **(b)** interaction between ionizing radiation, Hf-BPY-Fe, and the Fenton process at the mid-RT stage of full process radiosensitization.[29c] Adapted with permission. Copyright 2020, American Chemical Society.

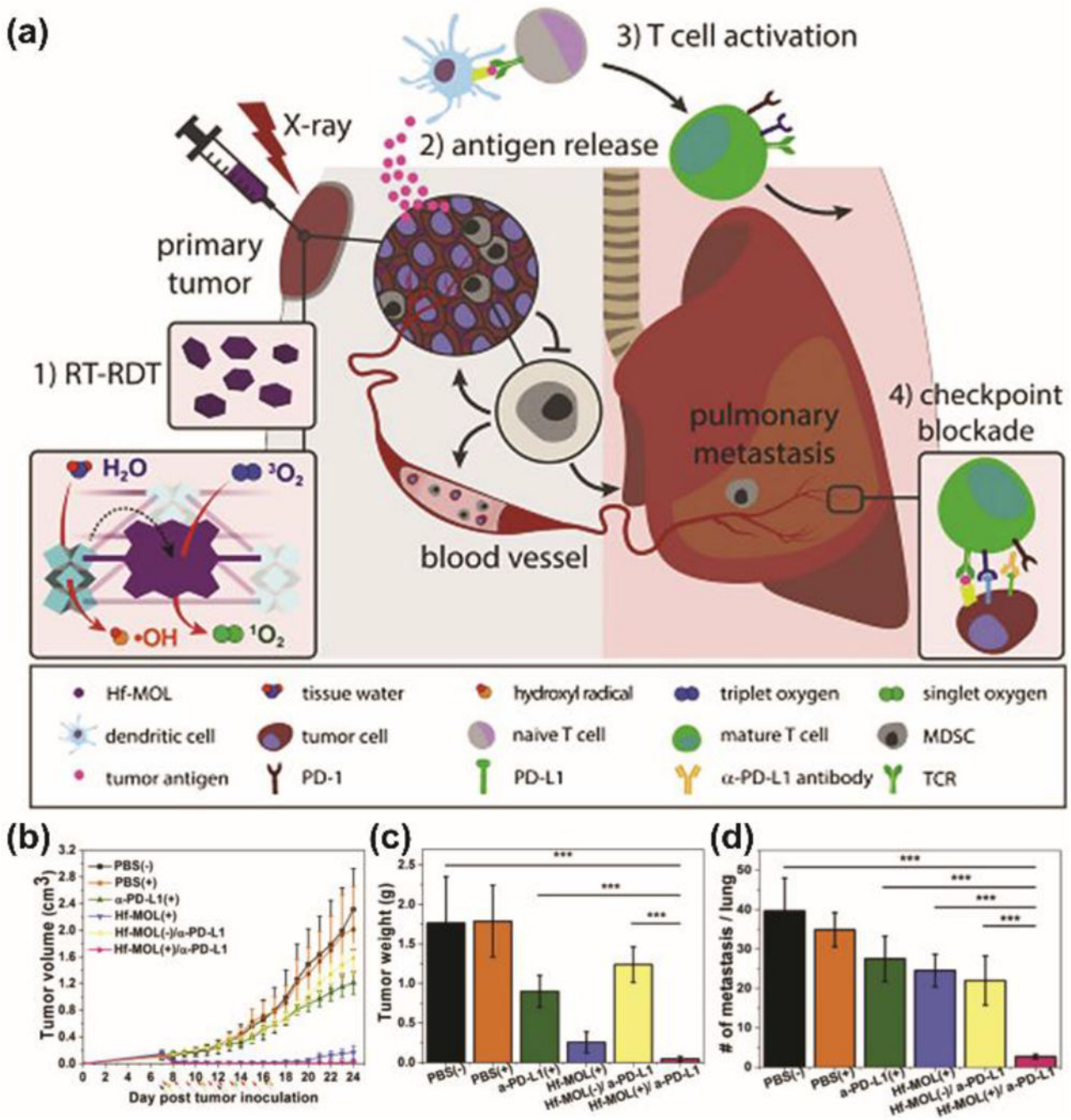

Figure 6.

(a) Hf-MOL enabled local RT-RDT treatment synergizes with CBI to elicit systemic antitumor and antimetastatic effects. **(b)** tumor growth curves, **(c)** weight, and **(d)** number of tumor nodules present in the lungs. Adapted with permission.[32] Copyright 2020, Cell Press.

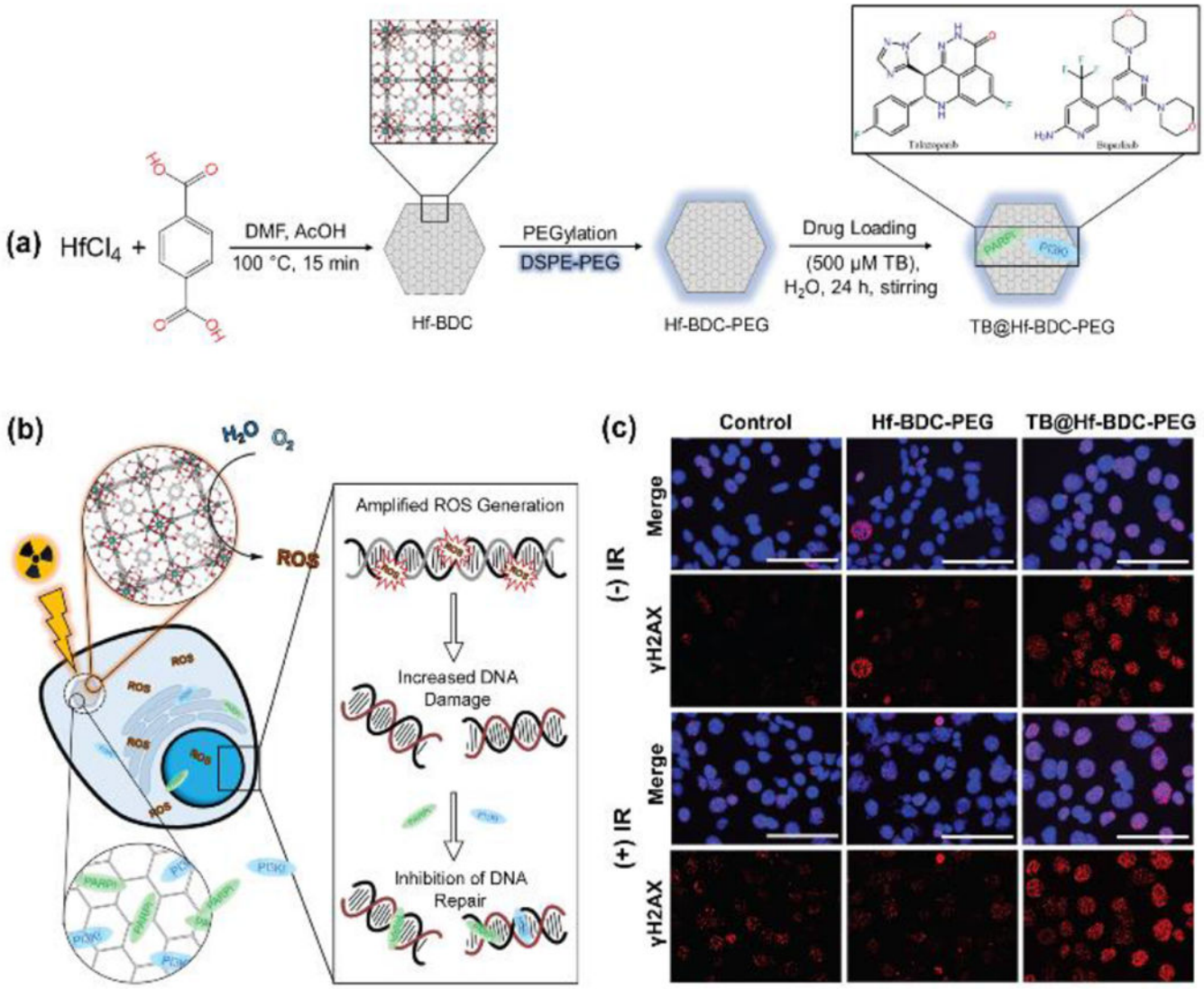

Figure 7.

(a) Synthesis route of TB@Hf-BDC-PEG and **(b)** mechanisms of therapeutic activity include radiosensitization through hafnium-mediated ROS enhancement following irradiation whereas the second mechanism involves the delivery of DNA damage repair (DDR) inhibitors. **(c)** Representative images of γH2AX foci in 4T1 cells treated with no drug, Hf-BDC-PEG, or TB@Hf-BDC-PEG and +/− RT. Nuclei were stained for DAPI (blue) and γH2AX (red). Scale bars represent 100 μm. Adapted with permission.[34] Copyright 2020, Springer.